Journal of proteome research

pubs.acs.org/jpr

Technical Note

Automated Phosphopeptide Enrichment for Gram-Positive Bacteria

Marlène S. Birk, Emmanuelle Charpentier, and Christian K. Frese*

Cite This: *J. Proteome Res.* 2021, 20, 4886–4892

Read Online

ACCESS | Metrics & More | Article Recommendations | Supporting Information

ABSTRACT: Protein phosphorylation in prokaryotes has gained more attention in recent years as several studies linked it to regulatory and signaling functions, indicating importance similar to protein phosphorylation in eukaryotes. Studies on bacterial phosphorylation have so far been conducted using manual or HPLC-supported phosphopeptide enrichment, whereas automation of phosphopeptide enrichment has been established in eukaryotes, allowing for high-throughput sampling. To facilitate the prospect of studying bacterial phosphorylation on a systems level, we here established an automated Ser/Thr/Tyr phosphopeptide enrichment workflow on the Agilent AssayMap platform. We present optimized buffer conditions for TiO_2 and Fe(III)-NTA-IMAC cartridge-based enrichment and the most advantageous, species-specific loading amounts for *Streptococcus pyogenes*, *Listeria monocytogenes*, and *Bacillus subtilis*. For higher sample amounts (≥250 μg), we observed superior performance of the Fe(III)-NTA cartridges, whereas for lower sample amounts (≤100 μg), TiO_2-based enrichment is equally efficient. Both cartridges largely enriched the same set of phosphopeptides, suggesting no improvement of peptide yield by the complementary use of the two cartridges. Our data represent, to the best of our knowledge, the largest phosphoproteome identified in a single study for each of these bacteria.

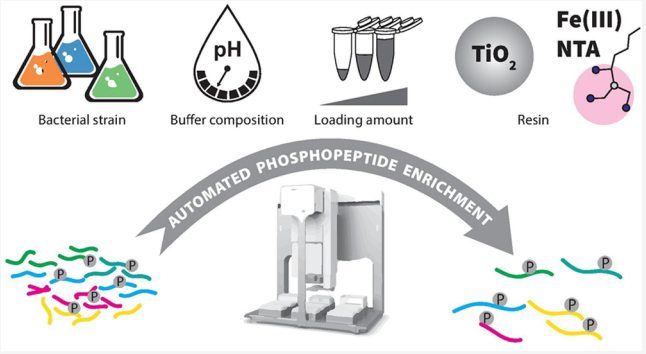

KEYWORDS: *BRAVO AssayMap, Fe(III)-IMAC, TiO_2, automation, phosphopeptide enrichment, Listeria monocytogenes, Bacillus subtilis, Streptococcus pyogenes, bacterial phosphoproteomics*

INTRODUCTION

Reversible phosphorylation is one of the most important post-translational modifications conserved in all domains of life.[1] Phosphorylation at serine (S), threonine (T), and tyrosine (Y) has been most comprehensively characterized and has been associated with numerous regulatory and signaling functions, particularly in eukaryotes. In recent years, evidence has accumulated suggesting that S/T/Y phosphorylation is, albeit at a less frequent occurrence, similarly important in prokaryotes.[2−4] A large subset of phosphorylated proteins in bacteria is involved in the central carbon metabolism.[5] Furthermore, protein phosphorylation in bacteria mediates different cellular processes required for virulence, including remodeling of the bacterial cell surface, expression of virulence genes, and interference with host signaling pathways.[6,7] Given the key role of bacterial phosphorylation in a variety of cellular processes, a fundamental understanding of these processes at the molecular level is important, providing essential insight into bacterial adaptation mechanisms. In particular, phosphoproteomic studies in bacterial pathogens can provide the framework to investigate the involvement of kinases and phosphatases in virulence and their potential as targets for drug development.

Mass spectrometry (MS)-based techniques have become the method of choice for phosphoproteomic analysis.[8] However, the substoichiometric nature of protein phosphorylation requires an effective phosphopeptide enrichment method prior to MS analysis. Common enrichment methods exploit the affinity of negatively charged phosphopeptides toward the positively charged metal ions (immobilized metal affinity chromatography; IMAC), such as Fe(III), or metal oxides (metal oxide affinity chromatography; MOAC), such as TiO_2.

Automated sample preparation is increasingly implemented into proteomic workflows in order to improve throughput, robustness, and reproducibility. Automation is particularly useful for laborious and error-prone multistep protocols such as phosphopeptide enrichment. In recent studies, an automated setup was used for phosphopeptide enrichment from eukaryotic cell culture, human cancer tissue, and primary neuronal cells from rats.[9−11] However, studies of bacterial phosphorylation have so far been conducted using manual or HPLC-supported phosphopeptide enrichment.[12] The establishment of automated phosphopeptide enrichment for

Received: April 30, 2021
Published: September 2, 2021

bacteria would allow for high-throughput sampling of multiple perturbations and/or temporal progression after a perturbation. Such a setup is required to obtain a systems-level view of protein phosphorylation-mediated adaptation mechanisms in bacteria.

Here, we established an automated Ser/Thr/Tyr phosphopeptide enrichment workflow on the Agilent AssayMap platform. We optimized the assay buffer conditions for two distinct enrichment strategies (TiO_2 and Fe(III)-NTA-IMAC) and evaluated phosphopeptide enrichment for different amounts of starting material from two pathogenic bacterial strains, *Streptococcus pyogenes* and *Listeria monocytogenes*, and the model organism *Bacillus subtilis*. Overall, our data revealed a superior performance of Fe(III)-NTA cartridges compared to TiO_2-based enrichment for higher sample amounts (≥250 μg). The optimal starting amount for Fe(III)-NTA cartridges was species-specific with the largest amount (1 mg) required for *B. subtilis* but only 500 μg for both *S. pyogenes* and *L. monocytogenes*. However, in the case of TiO_2 cartridges, we observed optimal yield from starting amounts of approximately 100 μg irrespective of the bacterial species. In total, we identified 449 unique phosphosites in *S. pyogenes*, 420 in *L. monocytogenes*, and 214 in *B. subtilis*. Our data represent, to the best of our knowledge, the largest phosphoproteome identified by a single study for each of these bacteria.

EXPERIMENTAL SECTION

Bacterial Culture

The bacterial strains used in this study are listed in supplementary Table S1. *L. monocytogenes* EGDe and *B. subtilis* were grown overnight at 37 °C with agitation at 180 rpm in 50 mL of brain heart infusion (BHI) and Lennox broth (LB), respectively. *S. pyogenes* was grown overnight in 50 mL of Todd Hewitt broth (THB) without shaking at 37 °C and 5% CO_2. Cultures were diluted 1/100 and grown under the above conditions for 6 h until stationary phase was reached. Bacteria were harvested by centrifugation (15 min, 4000*g* at 4 °C), and the supernatant was subsequently removed. The pellets were washed twice with cold DPBS, shock frozen in liquid nitrogen, and stored at −80 °C.

Cell Lysis

For bacterial cell lysis, 1 volume of bacteria pellet was resuspended in 5 volumes of lysis buffer (100 mM Tris-HCl pH 7.5, 4% SDS, 1% NP-40, 10 mM tris(2-carboxyethyl)-phosphine (TCEP), 40 mM 2-chloroacetamide (CAA), 1× complete protease inhibitor cocktail (Roche), 1× Halt phosphatase inhibitor cocktail (Thermo Fischer Scientific), 0.05 mg/mL Lysozyme). Samples were incubated at 95 °C for 10 min and subsequently cooled on ice for 10 min. Samples were placed on ice and lysed by sonication for 30 min (amplitude: 35%; 5 s on, 10 s off) using a SONOPULS HD 4100 (probe: TS 103; Bandelin). One thousand units of benzonase, $MgCl_2$ (final concentration 1 mM), and lysozyme (final concentration 0.1 mg/mL) were added to each sample. Samples were incubated for 1 h at 37 °C with agitation at 180 rpm. Cell debris was removed by centrifugation at 13,000*g* for 15 min at 4 °C.

Protein Digestion

Subsequently, acetone precipitation was performed by adding 4 volumes of acetone (−20 °C) to each sample. A 15 min incubation step at −80 °C was followed by 90 min incubation at −20 °C. Proteins were pelleted by centrifugation at 13,000*g* for 15 min at 4 °C. The pellet was washed three times with acetone (−20 °C) and air-dried prior to resuspension in 1 pellet volume of 8 M guanidine hydrochloride. Protein concentration was determined via micro-BCA protein assay (Thermo Fischer Scientific). The sample was then diluted to decrease the guanidine hydrochloride concentration to 1.5 M using 50 mM HEPES pH 8 containing Halt phosphatase inhibitor cocktail. Protein digestion was performed at 37 °C for 14 h using a mixture of trypsin and Lys-C at an enzyme-to-protein ratio of 1:50 and 1:100 (w/w), respectively. Protein digests were acidified to a final concentration of 1% formic acid (Sigma-Aldrich), and the precipitate was removed by centrifugation (13,000*g*, 10 min). Peptides were desalted using C18 Sep-Pak (3 cc) columns (Waters). The peptide concentration of the eluate was determined using the Pierce quantitative colorimetric peptide assay. The desired amounts of peptides were transferred to a 96-well plate, dried, and resuspended in phosphopeptide loading buffers as indicated. All enrichments were performed in duplicate per condition.

Phosphopeptide Enrichment

All phosphopeptide enrichment experiments were performed on an AssayMAP liquid handling platform (Agilent) using the "Phospho Enrichment v2.0" protocol with two types of cartridges available for the AssayMAP, TiO_2, and Fe(III)-IMAC. The buffer compositions for phosphopeptide enrichment are listed in supplementary Tables S2 and S3. For phosphopeptide enrichments, different amounts of desalted peptides were resuspended in 105 μL of the corresponding loading buffers. The cartridges were primed using 100 μL of the corresponding buffers from Table S2 and S3 at a flow rate of 300 μL/min and equilibrated with 50 μL of equilibration and wash buffer at 10 μL/min. Peptides were loaded onto the cartridge at a flow rate of 5 μL/min. The cartridges were washed three times with 50 μL of equilibration and wash buffer at 10 μL/min, and the phosphorylated peptides were eluted with 20 μL of elution buffer directly into 20 μL of neutralizing solvent at 5 μL/min. Samples were stored at −80 °C until analysis by LC-MS/MS.

LC-MS

All samples were analyzed on an Orbitrap Exploris 480 or Orbitrap Fusion Lumos (both Thermo Scientific), which were both equipped with a FAIMS Pro device and coupled to 3000 RSLC nano UPLC (Thermo Scientific). Samples were loaded on a pepmap trap cartridge (300 μm i.d. × 5 mm, C18, Thermo) with 2% acetonitrile and 0.1% TFA at a flow rate of 20 μL/min. Peptides were separated over a 50 cm analytical column (Picofrit, 360 μm o.d., 75 μm i.d., 10 μm tip opening, non-coated, New Objective) that was packed in-house with Poroshell 120 EC-C18, 2.7 μm (Agilent). Solvent A consists of 0.1% formic acid in water. Elution was carried out at a constant flow rate of 250 nL/min within 90 min. A two-step linear gradient was applied: 3−30% solvent B (0.1% formic acid in 80% acetonitrile) within 74 min, 30−45% solvent B within 14 min, followed by column washing and equilibration. The spray voltage was set to 2.2 kV. The ion transfer tube temperature was set to 275 °C. A survey MS1 scan was acquired from m/z 375−1500 at a resolution of 60,000. The normalized AGC target was set to 300%. Monoisotopic precursor selection was activated. Precursor ions with charge states 2−6 were isolated within a 1.4 Da window and subjected to HCD fragmentation (normalized collision energy 28%). The normalized AGC

https://doi.org/10.1021/acs.jproteome.1c00364
J. Proteome Res. 2021, 20, 4886−4892

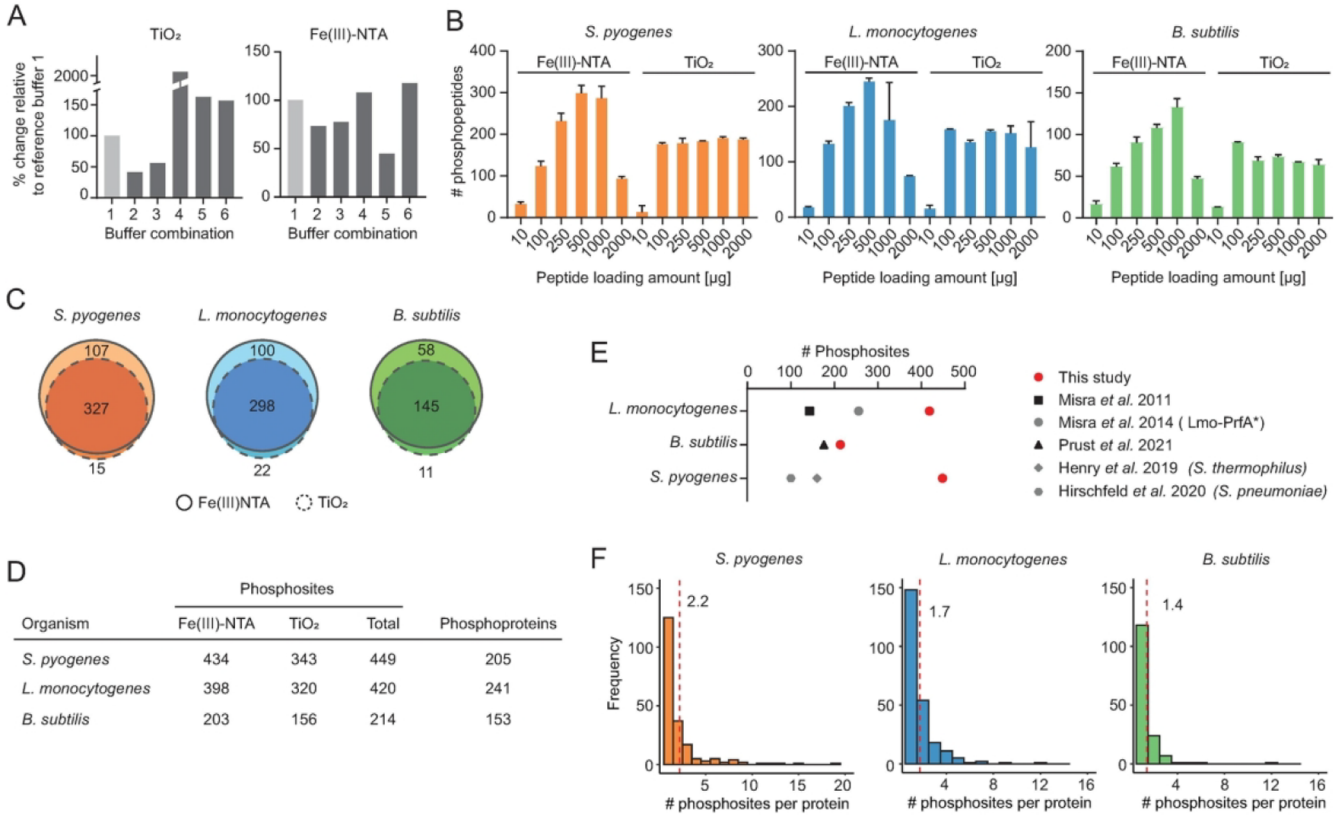

Figure 1. Automated enrichment of bacterial phosphopeptides using TiO_2 and Fe(III)-NTA cartridges on an Agilent AssayMAP platform. (A) Six different sets of buffers were evaluated for both resins using digests of *S. pyogenes*. Data are based on two replicate enrichments per buffer condition. See supplementary Tables S2 and S3 for exact buffer composition. (B) Number of phosphopeptides identified from each bacterial strain using an increasing amount of peptides. Data represent the mean and standard deviation of two independent enrichment procedures. (C) Overlap of identified phosphosites between TiO_2 and Fe(III)-NTA cartridges. (D) Total number of phosphosites and phosphoproteins identified from the three bacterial strains. (E) Comparison of these data to relevant related studies (Misra et al.,[20,21] Prust et al.,[12] Henry et al.,[22] and Hirschfeld et al.[23]). (F) Histograms illustrating the distribution of the number of phosphosites per protein. The dashed red line indicates the mean.

target was set to 200%, and the maximum injection time was set to 54 ms. MS2 scans were acquired at a resolution of 30,000. The cycle time was set to 1 s for each of the two FAIMS voltages of −45 and −65 V.

DDA Data Analysis

We retrieved the Uniprot protein databases containing canonical sequences for proteins from *B. subtilis* (14. June 2019; 4312 sequences), *S. pyogenes* (05. April 2019; 1691 sequences), and *L. monocytogenes* (19. February 2019; 2860 sequences). A database containing common contaminants was obtained from Maxquant. Raw files were converted into MzXML files[13] and then analyzed by Maxquant 1.6.14.0 using default settings. Trypsin/P was set as enzyme with a maximum of two cleavages. Oxidation (M) and phosphorylation (STY) were used as variable modification, and carbamidomethylation (C) was used as fixed modification. The "match-between-runs" option was enabled. Default parameters were used unless specified otherwise. The resulting txt files were further processed in Perseus 1.6.2.3 and R. Proteins flagged as "Reversed" and "Potential contaminant" were removed from the data set. Phosphosites with a localization probability of at least 0.75 were used for further analysis. For buffer comparison, peptides with at least one valid value per buffer condition (two technical replicates) were considered. For comparison of the different loading concentrations, peptides with at least two valid values in at least one concentration were considered. For all further analysis, peptides with at least two valid values per resin were considered. Data visualization was done using Graphpad Prism software and R with the ggplot2 package (https://ggplot2.tidyverse.org). Venn diagrams were created using the BioVenn web application.[14] Pathway analysis was done using the functional annotation clustering tool from the DAVID bioinformatics resources web application.[15,16] For analysis of potential motifs and conserved amino acids in the proximity of the phosphorylation site, we utilized pLogo web application[17] using FASTA files containing NCBI reference sequences (*L. monocytogenes*: NC_003210.1; *B. subtilis*: NC_000964.3; *S. pyogenes*: NZ_CP010450.1) as background. Proteins found to be phosphorylated in all three bacteria were searched using BlastP (https://blast.ncbi.nlm.nih.gov/Blast.cgi?PAGE=Proteins) against the "Model Organisms (landmark)" database. For human, yeast, and *Escherichia coli*, the highest scoring homologue was used for sequence alignment by Clustal Omega (https://www.ebi.ac.uk/Tools/msa/clustalo/).

Data Availability

The mass spectrometry proteomics data have been deposited to the ProteomeXchange Consortium via the PRIDE[18] partner repository with the data set identifier PXD025459.

https://doi.org/10.1021/acs.jproteome.1c00364
J. Proteome Res. 2021, 20, 4886−4892

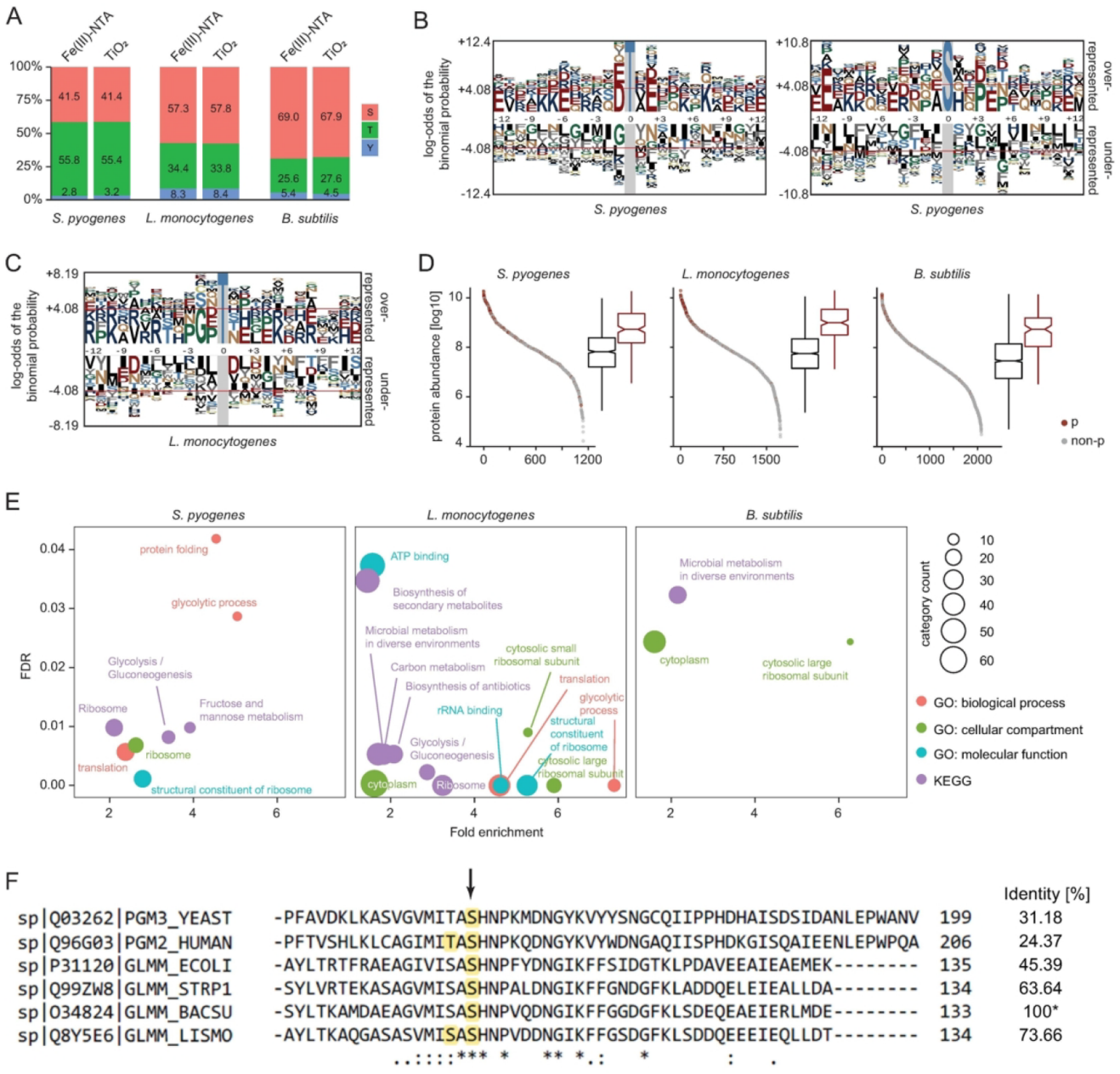

Figure 2. Analysis of phosphorylation in Gram-positive bacteria. (A) Distribution of S/T/Y phosphorylation sites. (B,C) Threonine and serine phosphorylation motif analyses for *S. pyogenes* (B) and threonine phosphorylation motif analyses for *L. monocytogenes* (C) using pLogo. (D) Analysis of phosphorylation in the context of the abundance of phosphoproteins in the cellular proteome. Dark red colored circles indicate if a protein was found to be phosphorylated. Box plots illustrate the abundance distribution of phosphoproteins (dark red) and nonphosphoproteins (black). The notch indicates the median. Outliers are not plotted. (E) KEGG and gene ontology enrichment analysis of the identified phosphoproteins. (F) Conservation analysis of phosphoglucomutase *glmM*. Sequence alignment reveals a high degree of conservation around the active site (arrow). Identified phosphosites are highlighted in yellow. Protein sequence identity relative to *B. subtilis* (*) as determined by BlastP.

RESULTS AND DISCUSSION

This study aimed to establish automated phosphopeptide enrichment from Gram-positive bacteria using the Agilent AssayMAP platform. As a first step, we evaluated a variety of different buffer combinations for use with the two types of cartridges available for the AssayMAP, TiO_2, and Fe(III)-IMAC. To this end, a whole-cell lysate of *S. pyogenes* was digested with trypsin and Lys-C. For each condition, 250 μg of peptides was subjected to TiO_2- and Fe(III)-IMAC-based automated phosphopeptide enrichment using different combinations of prime, loading, and wash buffers (Tables S2 and S3). Enriched phosphopeptides were subsequently analyzed by LC-MS/MS. The performance of each buffer combination was benchmarked against a commonly used set of buffers as published by Post et al.[9]

For TiO_2, we detected the highest number of phosphosites using the glycolic acid-containing loading buffer described by Palmisano et al.[19] (buffer 4 Table S2). The superior yield can be attributed to the higher proportion of trifluoroacetic acid (TFA) and the use of multifunctional glycolic acid. For the Fe(III)-IMAC cartridges, we identified the highest number of phosphosites using buffer set 6 (Table S3). Here, in contrast to

https://doi.org/10.1021/acs.jproteome.1c00364
J. Proteome Res. 2021, 20, 4886−4892

the default set of buffers, cartridge equilibration and washing were carried out using a lower amount of organic solvent (50 vs 80% acetonitrile) at a slightly higher pH (0.1% acetic acid vs 0.1% TFA) (Figure 1A). Additionally, 0.1% TFA in 50% acetonitrile was used for cartridge priming instead of 0.1% TFA in water.

Having established the optimal buffers for each of the two cartridges, we focused on evaluating the amount of peptides to be loaded onto the cartridges for maximum phosphopeptide yield. Due to the differences in binding capacity of the resins and the differences in genome size and number of kinases and phosphatases between bacterial strains, we optimized the loading amount separately for each of the three Gram-positive bacteria and both cartridges. Six different amounts ranging from 10 to 2000 μg peptides derived from *S. pyogenes*, *L. monocytogenes*, and *B. subtilis* were subjected to either TiO_2- or Fe(III)-IMAC-based automated phosphopeptide enrichment using the optimized buffers (Figure 1B). Enriched phosphopeptides were subsequently analyzed by LC-MS/MS on an Orbitrap Exploris 480. Utilizing Fe(III)-IMAC cartridges, the best results for *L. monocytogenes* and *S. pyogenes* were obtained when using 500 μg of peptides for enrichment. Notably, a higher starting amount (1 mg) was required for optimal phosphopeptide yield from *B. subtilis*. In the case of TiO_2, we observed an increase in the number of identified unique phosphosites from 10 to 100 μg starting material for all three bacteria. However, amounts above 100 μg did not significantly improve the yield. Intriguingly, the TiO_2 cartridges gave a yield slightly higher than that of the Fe(III)-IMAC cartridges for all three bacterial strains when using only 100 μg of peptides as input. This indicates that TiO_2 cartridges might be suitable for effective enrichment of phosphopeptides from Gram-positive bacteria when the starting material is limited to 100 μg, whereas Fe(III)-IMAC enrichment would be the preferred resin in scenarios where sample availability is not the limiting factor. Note that the overall enrichment efficiency was highest for *S. pyogenes* (22× more phosphopeptides than input) and lowest for *B. subtilis* (8× more phosphopeptides than input) (Figure S1).

Next, we aggregated the phosphosites identified for each bacterial strain and for both resins. Overall, Fe(III)-IMAC-based enrichment outperformed the TiO_2-based workflow, identifying approximately 20% more phosphosites (*S. pyogenes* +20.8%, *B. subtilis* +23.2%, and *L. monocytogenes* +19.6%). The overall lower performance of the TiO_2 automated workflow on the AssayMAP platform was expected, as Post et al.[9] demonstrated a similar decreased performance of TiO_2 for phosphopeptide enrichment from mammalian samples. We observed that TiO_2 and Fe(III)-IMAC largely enrich the same set of phosphopeptides (Figure 1C), indicating that the complementary use of both cartridges does not improve the overall outcome. In total, we identified 449 phosphosites in *S. pyogenes*, 420 in *L. monocytogenes*, and 214 in *B. subtilis* (Figure 1D and Supporting Information). This represents the largest phosphoproteome reported for either bacterium for a single growth condition (Figure 1E).[12,20,21] Note that in the case of *S. pyogenes*, no phosphoproteomic analysis has been performed to date. We therefore compared our data set to studies performed on the closely related strains *Streptococcus thermophilus*[22] and *Streptococcus pneumoniae*.[23]

The 449 unique phosphosites in *S. pyogenes* are derived from 205 phosphoproteins (2.2 phosphosites per phosphoprotein). In *L. monocytogenes* (241 phosphoproteins; 1.7 phosphosites per protein) and *B. subtilis* (153 phosphoproteins; 1.4 phosphosites per protein), we observed a lower phosphorylation frequency (Figure 1F).

Next, we asked to which extent the phosphosite distribution would vary between bacterial strains. While the distribution of S/T/Y phosphorylation was nearly identical between cartridges, we observed large variation between bacterial strains. *B. subtilis* and *L. monocytogenes* showed the highest percentage of phosphorylation at serine followed by threonine and tyrosine (S/T/Y 67/28/5% for *B. subtilis* and 56/35/9% for *L. monocytogenes*). Our data are in line with previously reported S/T/Y phosphorylation−distribution in *B. subtilis* and *L. monocytogenes*, approximately 70/20/10%[2,24,25] and 65/30/5%,[2,20,21] respectively. Notably, we observed that threonine was the main site of phosphorylation in *S. pyogenes* (Figure 2A). We observed a S/T/Y phosphorylation distribution of approximately 41/55/4% in *S. pyogenes*, which is different from the reported distributions in two closely related species, *S. pneumoniae* and *S. thermophilus* (approximately 47/44/9% and 43/33/23%, respectively).[2,22,26]

Next, we sought out to identify specific motifs and conserved amino acids adjacent to the phosphorylation sites. We analyzed the enriched motifs in the flanking regions of phosphorylated S, T, and Y (pS, pT, and pY) using pLogo.[17] For *S. pyogenes*, we observed enrichment of proline at position 3 upstream of pS and a higher frequency of glutamic acid and aspartic acid adjacent to pT with an enriched motif at −1 and +2, respectively (Figure 2B). In *L. monocytogenes*, we observed enrichment of glycine at position 2 downstream of pT (−2) (Figure 2C). No distinct motif was observed for *B. subtilis*.

Involvement of protein phosphorylation in the regulation of the central carbon metabolism was proposed in previous studies as a large subset of phosphorylated proteins in bacteria is involved in this pathway.[2,5,20,24,27] In line with those findings, gene ontology enrichment analysis revealed enrichment of phosphoproteins involved in carbohydrate metabolism in *L. monocytogenes* and *S. pyogenes*. Additionally, we observed enrichment of proteins involved in translation in all three species (Figure 2E). As those proteins are rather abundant in the cell, we next asked to which extend we can identify phosphorylation sites from lower abundant proteins (Figure 2D). In line with our expectations, we found that the majority of the identified phosphosites are derived from highly abundant phosphoproteins. However, we also detected phosphopeptides from lower abundant proteins.

For conservation analysis between the phosphoproteomes of *S. pyogenes*, *L. monocytogenes*, and *B. subtilis*, we matched identified phosphoproteins based on their gene name and found 10 phosphoproteins common to all three bacterial strains (*glmM*, *ptsH*, *gpsB*, *dnaK*, *groL*, *groS*, *tuf*, *rpoB*, *rplJ*, and *pgi*). We performed a BlastP search to identify interspecies homologues. The highest scoring homologue for human, yeast, and the Gram-negative *E. coli* was used for sequence alignment. A conserved serine phosphorylation site for all six organisms was found for the evolutionarily conserved bacterial enzyme phosphoglucosamine mutase (PNGM/GlmM), which participates in the cytoplasmic steps of peptidoglycan biosynthesis (Figure 2F). The amino acid sequence covering the active site of GlmM is highly conserved across archaea, bacteria, and eukaryotes. Serine phosphorylation at the active site has already been demonstrated for *B. subtilis*, *E. coli*, and *Homo sapiens*.[27] Here, we provide evidence that phosphorylation at this serine also occurs in *S. pyogenes* and *L. monocytogenes*.

https://doi.org/10.1021/acs.jproteome.1c00364
J. Proteome Res. 2021, 20, 4886−4892

CONCLUSIONS

Bacterial post-translational modifications, in particular, phosphorylation, are increasingly becoming the focus of studies on virulence, adaptation, and host−pathogen interactions. To study bacterial phosphorylation by LC-MS/MS, an automated setup implementing otherwise laborious and error-prone multistep phosphopeptide enrichment protocols is key to improve throughput, robustness, and reproducibility. Here, we present an optimized workflow for species-specific TiO_2 and Fe(III)-NTA-IMAC-based phosphopeptide enrichment on the popular Agilent AssayMap liquid handling platform. Using this optimized approach, we generated the largest phosphoproteome based on a single growth condition for each of the tested bacteria. Note that phosphopeptide enrichment after offline HPLC-based peptide fractionation could further increase the depth of the phosphoproteome.[28] Our data suggest that the optimal phosphopeptide enrichment strategy is species-specific with different optimal starting amounts for different organisms and different cartridges depending on the available sample amount. We present the first global phosphoproteomic analysis of the human pathogen *S. pyogenes* and discovered differences to the phosphoproteome of closely related species. Despite possessing the smallest genome among the three tested organisms, we identified the largest number of phosphosites in *S. pyogenes* and discovered a higher phosphorylation frequency per phosphoprotein compared to that of *L. monocytogenes* and *B. subtilis*. We also observed a remarkably different S/T/Y phosphorylation distribution between *S. pyogenes* and the other two bacteria, with threonine being more frequently phosphorylated than serine in *S. pyogenes*. Additionally, our data revealed a higher frequency of glutamic acid and aspartic acid near pT in *S. pyogenes*, indicating a phosphorylation motif.

ASSOCIATED CONTENT

Supporting Information

The Supporting Information is available free of charge at https://pubs.acs.org/doi/10.1021/acs.jproteome.1c00364.

Analysis of phosphopeptide enrichment in Gram-positive bacteria (Figure S1); overview of the bacterial strains used in this study (Table S1); composition of the buffers evaluated for TiO_2 cartridges (Table S2); composition of the buffers evaluated for Fe(III)-NTA cartridges (Table S3) (PDF)

Summary of all identified phosphosites (XLSX)

AUTHOR INFORMATION

Corresponding Author

Christian K. Frese − *Max Planck Unit for the Science of Pathogens, 10117 Berlin, Germany;* orcid.org/0000-0001-7919-4642; Email: frese@mpusp.mpg.de

Authors

Marlène S. Birk − *Max Planck Unit for the Science of Pathogens, 10117 Berlin, Germany*

Emmanuelle Charpentier − *Max Planck Unit for the Science of Pathogens, 10117 Berlin, Germany*

Complete contact information is available at: https://pubs.acs.org/10.1021/acs.jproteome.1c00364

Funding

The authors would like to acknowledge funding from the Max Planck Society (to C.K.F. and E.C.).

Notes

The authors declare no competing financial interest.

ACKNOWLEDGMENTS

We thank Pascale Cossart for providing the *L. monocytogenes* EGD-e strain, Tim Clausen for providing *B. subtilis* 168 strain, and Siang-Wun Siao as well as Kathirvel Alagesan for critical reading of the manuscript.

REFERENCES

(1) Hunter, T. Why Nature Chose Phosphate to Modify Proteins. *Philos. Trans. R. Soc., B* **2012**, *367* (1602), 2513−2516.

(2) Yagüe, P.; Gonzalez-Quiñonez, N.; Fernández-García, G.; Alonso-Fernández, S.; Manteca, A. Goals and Challenges in Bacterial Phosphoproteomics. *Int. J. Mol. Sci.* **2019**, *20* (22), 5678.

(3) Macek, B.; Forchhammer, K.; Hardouin, J.; Weber-Ban, E.; Grangeasse, C.; Mijakovic, I. Protein Post-Translational Modifications in Bacteria. *Nat. Rev. Microbiol.* **2019**, *17* (11), 651−664.

(4) Mijakovic, I.; Grangeasse, C.; Turgay, K. Exploring the Diversity of Protein Modifications: Special Bacterial Phosphorylation Systems. *FEMS Microbiology Reviews* **2016**, *40* (3), 398−417.

(5) Kobir, A.; Shi, L.; Boskovic, A.; Grangeasse, C.; Franjevic, D.; Mijakovic, I. Protein Phosphorylation in Bacterial Signal Transduction. *Biochim. Biophys. Acta, Gen. Subj.* **2011**, *1810* (10), 989−994.

(6) Jers, C.; Soufi, B.; Grangeasse, C.; Deutscher, J.; Mijakovic, I. Phosphoproteomics in Bacteria: Towards a Systemic Understanding of Bacterial Phosphorylation Networks. *Expert Rev. Proteomics* **2008**, *5* (4), 619−627.

(7) Bonne Køhler, J.; Jers, C.; Senissar, M.; Shi, L.; Derouiche, A.; Mijakovic, I. Importance of Protein Ser/Thr/Tyr Phosphorylation for Bacterial Pathogenesis. *FEBS Lett.* **2020**, *594* (15), 2339−2369.

(8) Eyrich, B.; Sickmann, A.; Zahedi, R. P. Catch Me If You Can: Mass Spectrometry-Based Phosphoproteomics and Quantification Strategies. *Proteomics* **2011**, *11* (4), 554−570.

(9) Post, H.; Penning, R.; Fitzpatrick, M. A.; Garrigues, L. B.; Wu, W.; MacGillavry, H. D.; Hoogenraad, C. C.; Heck, A. J. R.; Altelaar, A. F. M. Robust, Sensitive, and Automated Phosphopeptide Enrichment Optimized for Low Sample Amounts Applied to Primary Hippocampal Neurons. *J. Proteome Res.* **2017**, *16* (2), 728−737.

(10) Abelin, J. G.; Patel, J.; Lu, X.; Feeney, C. M.; Fagbami, L.; Creech, A. L.; Hu, R.; Lam, D.; Davison, D.; Pino, L.; Qiao, J. W.; Kuhn, E.; Officer, A.; Li, J.; Abbatiello, S.; Subramanian, A.; Sidman, R.; Snyder, E.; Carr, S. A.; Jaffe, J. D. Reduced-Representation Phosphosignatures Measured by Quantitative Targeted MS Capture Cellular States and Enable Large-Scale Comparison of Drug-Induced Phenotypes. *Molecular & Cellular Proteomics* **2016**, *15* (5), 1622−1641.

(11) Murillo, J. R.; Kuras, M.; Rezeli, M.; Milliotis, T.; Betancourt, L.; Marko-Varga, G. Automated Phosphopeptide Enrichment from Minute Quantities of Frozen Malignant Melanoma Tissue. *PLoS One* **2018**, *13* (12), No. e0208562.

(12) Prust, N.; van der Laarse, S.; van den Toorn, H.; van Sorge, N. M.; Lemeer, S. In Depth Characterization of the Staphylococcus Aureus Phosphoproteome Reveals New Targets of Stk1. *Mol. Cell Proteomics* **2021**, *20*, 100034.

(13) Hebert, A. S.; Prasad, S.; Belford, M. W.; Bailey, D. J.; McAlister, G. C.; Abbatiello, S. E.; Huguet, R.; Wouters, E. R.; Dunyach, J.-J.; Brademan, D. R.; Westphall, M. S.; Coon, J. J. Comprehensive Single-Shot Proteomics with FAIMS on a Hybrid Orbitrap Mass Spectrometer. *Anal. Chem.* **2018**, *90* (15), 9529−9537.

(14) Hulsen, T.; de Vlieg, J.; Alkema, W. BioVenn - a Web Application for the Comparison and Visualization of Biological Lists Using Area-Proportional Venn Diagrams. *BMC Genomics* **2008**, *9*, 488.

(15) Huang, D. W.; Sherman, B. T.; Lempicki, R. A. Systematic and Integrative Analysis of Large Gene Lists Using DAVID Bioinformatics Resources. *Nat. Protoc.* **2009**, *4* (1), 44−57.
(16) Huang, D. W.; Sherman, B. T.; Lempicki, R. A. Bioinformatics Enrichment Tools: Paths toward the Comprehensive Functional Analysis of Large Gene Lists. *Nucleic Acids Res.* **2009**, *37* (1), 1−13.
(17) O'Shea, J. P.; Chou, M. F.; Quader, S. A.; Ryan, J. K.; Church, G. M.; Schwartz, D. PLogo: A Probabilistic Approach to Visualizing Sequence Motifs. *Nat. Methods* **2013**, *10* (12), 1211−1212.
(18) Perez-Riverol, Y.; Csordas, A.; Bai, J.; Bernal-Llinares, M.; Hewapathirana, S.; Kundu, D. J.; Inuganti, A.; Griss, J.; Mayer, G.; Eisenacher, M.; Pérez, E.; Uszkoreit, J.; Pfeuffer, J.; Sachsenberg, T.; Yilmaz, S.; Tiwary, S.; Cox, J.; Audain, E.; Walzer, M.; Jarnuczak, A. F.; Ternent, T.; Brazma, A.; Vizcaíno, J. A. The PRIDE Database and Related Tools and Resources in 2019: Improving Support for Quantification Data. *Nucleic Acids Res.* **2019**, *47* (D1), D442−D450.
(19) Palmisano, G.; Parker, B. L.; Engholm-Keller, K.; Lendal, S. E.; Kulej, K.; Schulz, M.; Schwämmle, V.; Graham, M. E.; Saxtorph, H.; Cordwell, S. J.; Larsen, M. R. A Novel Method for the Simultaneous Enrichment, Identification, and Quantification of Phosphopeptides and Sialylated Glycopeptides Applied to a Temporal Profile of Mouse Brain Development. *Molecular & Cellular Proteomics* **2012**, *11* (11), 1191−1202.
(20) Misra, S. K.; Milohanic, E.; Aké, F.; Mijakovic, I.; Deutscher, J.; Monnet, V.; Henry, C. Analysis of the Serine/Threonine/Tyrosine Phosphoproteome of the Pathogenic Bacterium Listeria Monocytogenes Reveals Phosphorylated Proteins Related to Virulence. *Proteomics* **2011**, *11* (21), 4155−4165.
(21) Misra, S. K.; Moussan Désirée Aké, F.; Wu, Z.; Milohanic, E.; Cao, T. N.; Cossart, P.; Deutscher, J.; Monnet, V.; Archambaud, C.; Henry, C. Quantitative Proteome Analyses Identify PrfA-Responsive Proteins and Phosphoproteins in *Listeria Monocytogenes*. *J. Proteome Res.* **2014**, *13* (12), 6046−6057.
(22) Henry, C.; Haller, L.; Blein-Nicolas, M.; Zivy, M.; Canette, A.; Verbrugghe, M.; Mézange, C.; Boulay, M.; Gardan, R.; Samson, S.; Martin, V.; André-Leroux, G.; Monnet, V. Identification of Hanks-Type Kinase PknB-Specific Targets in the Streptococcus Thermophilus Phosphoproteome. *Front. Microbiol.* **2019**, *10*, 1329.
(23) Hirschfeld, C.; Gómez-Mejia, A.; Bartel, J.; Hentschker, C.; Rohde, M.; Maaß, S.; Hammerschmidt, S.; Becher, D. Proteomic Investigation Uncovers Potential Targets and Target Sites of Pneumococcal Serine-Threonine Kinase StkP and Phosphatase PhpP. *Front. Microbiol.* **2020**, *10*, 3101.
(24) Macek, B.; Mijakovic, I.; Olsen, J. V.; Gnad, F.; Kumar, C.; Jensen, P. R.; Mann, M. The Serine/Threonine/Tyrosine Phosphoproteome of the Model Bacterium Bacillus Subtilis. *Mol. Cell Proteomics* **2007**, *6* (4), 697−707.
(25) Ravikumar, V.; Shi, L.; Krug, K.; Derouiche, A.; Jers, C.; Cousin, C.; Kobir, A.; Mijakovic, I.; Macek, B. Quantitative Phosphoproteome Analysis of Bacillus Subtilis Reveals Novel Substrates of the Kinase PrkC and Phosphatase PrpC. *Mol. Cell Proteomics* **2014**, *13* (8), 1965−1978.
(26) Sun, X.; Ge, F.; Xiao, C.-L.; Yin, X.-F.; Ge, R.; Zhang, L.-H.; He, Q.-Y. Phosphoproteomic Analysis Reveals the Multiple Roles of Phosphorylation in Pathogenic Bacterium *Streptococcus Pneumoniae*. *J. Proteome Res.* **2010**, *9* (1), 275−282.
(27) Macek, B.; Gnad, F.; Soufi, B.; Kumar, C.; Olsen, J. V.; Mijakovic, I.; Mann, M. Phosphoproteome Analysis of E. Coli Reveals Evolutionary Conservation of Bacterial Ser/Thr/Tyr Phosphorylation. *Molecular & Cellular Proteomics* **2008**, *7* (2), 299−307.
(28) Batth, T. S.; Francavilla, C.; Olsen, J. V. Off-Line High-PH Reversed-Phase Fractionation for in-Depth Phosphoproteomics. *J. Proteome Res.* **2014**, *13* (12), 6176−6186.

https://doi.org/10.1021/acs.jproteome.1c00364
J. Proteome Res. 2021, 20, 4886−4892